Nanocrystalline cerium oxide prepared from carbonate precursor and its ability to breakdown biologically relevant organophosphates

Pavel Janoš[1,], Jiří Henych[1,2], Jan Pfeifer[1], Nikola Zemanová[1], Věra Pilařová[1], David Milde[3], Tomáš Opletal[3], Jakub Tolasz[2,4], Marek Malý[4], Václav Štengl[2]*

[1] Faculty of the Environment, University of Jan Evangelista Purkyně, Králova Výšina 7, 400 96 Ústí nad Labem, Czech Republic
[2] Institute of Inorganic Chemistry AS CR v.v.i., 25068 Řež, Czech Republic
[3] Palacký University, Regional Centre of Advanced Technologies and Materials, Department of Analytical Chemistry, Faculty of Science, Palacký University, 17. listopadu 12, CZ 771 46 Olomouc, Czech Republic
[4] Faculty of Sciences, University of Jan Evangelista Purkyně, České Mládeže 8, 400 96 Ústí nad Labem, Czech Republic

Electronic Supporting Information

Content

S1. Preparation of cerium oxide

a) Homogeneous precipitation with urea

In a typical arrangement, cerium oxide was prepared by homogeneous precipitation as follows: 30 g $Ce(NO)_3 \cdot 6\ H_2O$ was dissolved in deionized water, acidified with 10 mL of concentrated nitric acid and diluted to 4 L with distilled water. Urea (150 g) was added in several portions and the mixture was heated at (90±2) °C under stirring until pH reached 7 and a white precipitate appeared, then the stirring continued for additional 2 hours. Finally, the mixture was left to stay until the next day; the precipitate was decanted, filtered and dried at 105 °C. Cerium oxide was prepared by annealing at 500 °C for 2 hours and further denoted as **HP-CeO_2**.

Some operational parameters were varied during an optimization of the preparation route:

i) Source of Ce^{3+}: Identical results were obtained, when cerium (III) chloride was used instead of cerium (III) nitrate. On the other hand, a utilization of cerium sulphate (or other sulphate salts or H_2SO_4) is not recommended because of a risk of a precipitation of sparingly soluble salts and a tendency to incorporate foreign ions into the precipitate.

ii) The initial concentrations of the Ce^{3+} varied in the range of ca. 0.01 to 0.06 mol/L, whereas the concentration of urea ranged from ca. 0.5 to 2.0 mol/L. At lower initial concentrations of the Ce^{3+} ions, almost monodisperse, isolated needle-like particles originated, whereas at high concentrations of the Ce^{3+} ions, more complex irregular clusters were formed. The concentration of urea did not affect the shape and size of the precipitated particles providing that it is present in a sufficient excess.

iii) Temperature during the precipitation was kept in the range of 90±2 °C. None detectable effect on the particle shapes or sizes was observed, when temperature dropped to 88 °C or increased to 95 °C. An initial amount of nitric acid affected the time period before the first precipitated particles appeared, but not influenced the morphology of the particles (assuming, of course, that the precipitation starts from the acid solution).

The changes in the particle sizes and shapes with increasing concentration of the Ce^{3+} ions are demonstrated in Fig. S1.

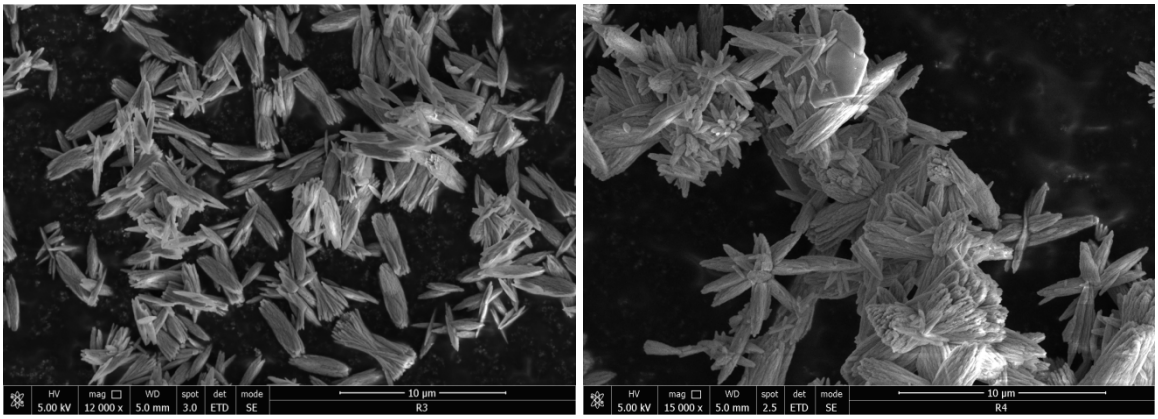

a) b)

Fig. S1. Cerium carbonate prepared by homogeneous precipitation with urea. Initial concentrations of the Ce^{3+} ions: a) 0.017 mol/L; b) 0.058 mol/L

b) Precipitation with aqueous ammonium bicarbonate (conventional precipitation/calcination method)

The carbonate precursor was prepared by precipitation of an aqueous solution of cerous nitrate (0.2 mol/L) with an excess of ammonium bicarbonate (0.5 mol/L) under stirring; the completeness of the precipitation was checked by reaction with oxalic acid. After adding the last portion of ammonium bicarbonate, the agitation continued for one more hour and the precipitate was left until the following day. Then, the precipitate was separated by filtration, washed with water, and dried overnight at 105° C. Cerium oxide was prepared by annealing at 500 °C for 2 hours and further denoted as **CA-CeO_2**.

For comparison, a commercially available nanocrystalline cerium oxide **MKN-0250** (MKnano, Missisauga, USA) was involved in the study.

S2. SEM images

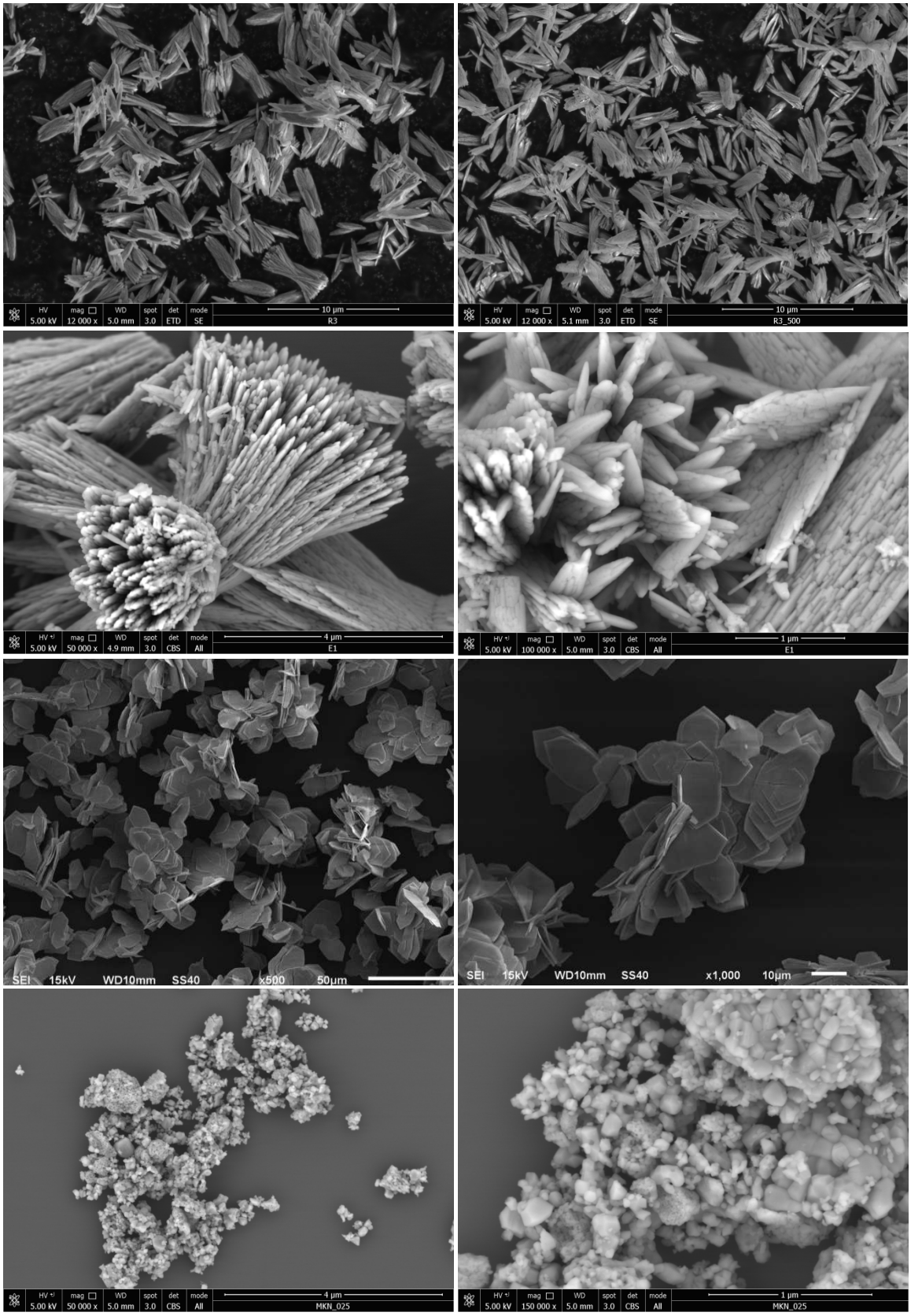

Fig. S2. a) Cerium carbonate prepared by homogeneous precipitation with urea, dried at 105 °C; b) – d) cerium oxide prepared by annealing from this cerium carbonate (HP-CeO_2); e) and f) cerium oxide prepared by conventional precipitation/calcination (CA-CeO_2) ; g) and h) commercial nanoceria MKN-025

The white or pale yellow precipitate obtained by homogeneous precipitation from the cerium nitrate solution using urea as the precipitant consisted of the uniformly-sized bundle-like aggregates with a typical length of ca. 5 µm and a typical diameter of 1 – 3 µm (see Fig. S2a). The sizes and shapes of the aggregates do not change during the thermal treatment, and thus the cerium oxide obtained by annealing from this precursor (HP-CeO_2) retained nearly the same morphology (Fig. S2b). As can be seen from a more detailed inspection, the bundle-like aggregates obtained by homogeneous precipitation are formed from bunches of thin nanorods or narrow and thin nanoplates, sometimes sharpened like a spear or lance (Fig. S2c,d). A typical thickness of these nanorods or nanoplates was several nanometers, and their more complex sub-micrometer structure is clearly visible in Fig. S2d. The cerium oxide prepared by a more conventional precipitation/calcination method (CA-CeO_2), on the other hand, exhibits a quite different morphology (Fig. S1e,f) with a typical diameter of the flower-like aggregates of ca. 10 µm. The commercial nanoceria MKN-025 consists of individual sub-micrometer "primary particles" only poorly assembled together, and its nanocrystalline structure is clearly visible from Figs S2 g,h.

The bundle-like morphology is characteristics for carbonates (and consequently oxides) of other rare-earth elements prepared in a similar way, as shown in Fig. S3.

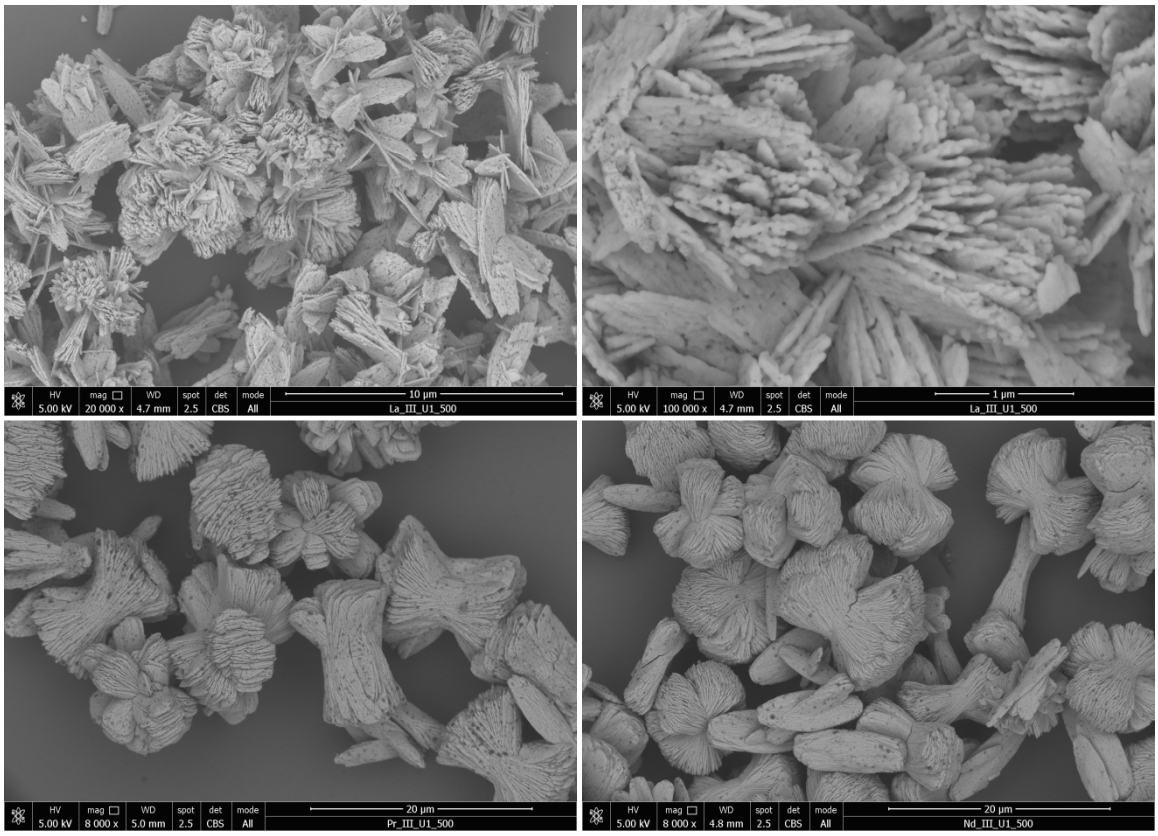

Fig. S3. a) - b) Lanthanum oxide; c) Praseodymium oxide; d) Neodymium oxide. All samples prepared in a similar way, as the HPnCe cerium oxide

S3. Thermogravimetric analysis

It is assumed that both precursors (prepared by homogeneous precipitation with urea and by conventional precipitation with ammonium bicarbonate) consist mainly of basic cerium carbonates, which composition may be approximated by the formula $Ce(OH)CO_3$. Similar patterns were obtained during the thermogravimetric analysis (Fig. S4). In the temperature range about 150°C, the first step of dehydration occurs, when poorly retained water molecules are liberated, whereas the decarboxylation (the liberation of CO_2) occurs at temperatures about 250 – 280°C. Although the main changes in the sample weight finished at the temperature about 300°C, a complex set of chemical changes and phase transformations continued with increasing temperature involving further decarboxylation and oxidation of trivalent cerium to tetravalent, removal of residual -OH groups and (re)crystallization of CeO_2-based solid solutions. It should be pointed out that the removal of the residual -OH groups requires the temperatures as high as 800°C [1, 2]. The total weight losses estimated from the TG curves (ca. 23 and 25 %, respectively) are in a good agreement with the theoretical value for the $Ce(OH)CO_3 \rightarrow CeO_2$ transformation (22.1%).

° C

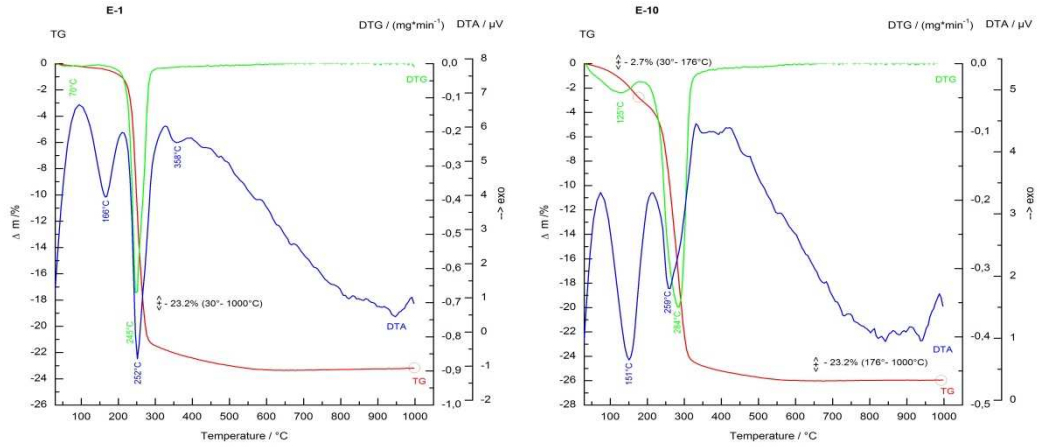

Fig. S4. Thermogravimetric analyses of the cerium carbonate precursors: a) Prepared by homogenous precipitation with urea; b) Prepared by conventional precipitation with ammonium bicarbonate

References

[1] Savin, V.D., Sobolev, V.N., Eremenko, Z.V., Grigor'eva, Z.M., Thermochemical investigations of cerium carbonate decomposition. *Zhurnal Fiz. Khimii* 1985, *59*, 571–575.

[2] Kosynkin, V.D., Arzgatkina, A.A., Ivanov, E.N., Chtoutsa, M.G., et al., The study of process production of polishing powder based on cerium dioxide. *J. Alloys Compd.* 2000, *303–304*, 421–425.

S4. Some physico-chemical characteristics of cerium oxides

Table S1. Physico-chemical characteristics of cerium oxides

Sample	Crystallite size (nm)	Total surface area (m^2/g)	Total pore volume (mL/g)	Micropore surface area (m^2/g)	Micropore volume (mL/g)	PZC[a)]
HP-CeO_2	12.3	97.7	0.098	33.1	0.0146	5.95
CA-CeO_2	13.0	65.5	0.067	24.3	0.0106	6.03
MKN-025	62.6	6.8	0.062	<0.1	<0.0005	6.22

[a)] PZC – point of zero charge

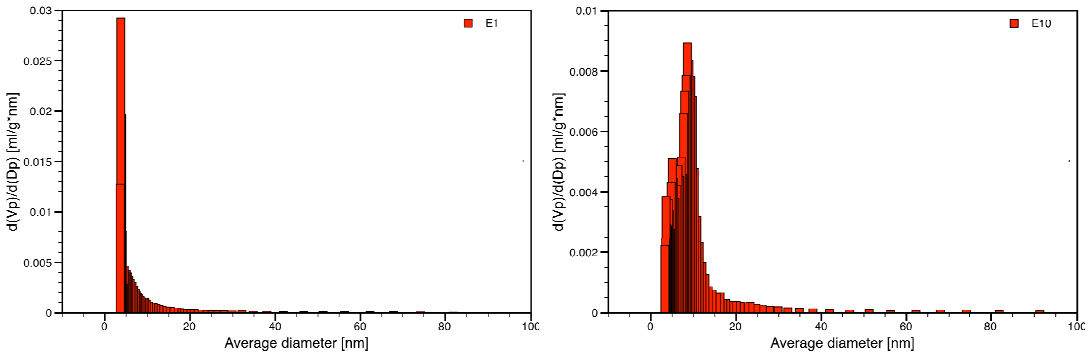

a) b)

Fig. S5. Pore size distributions. a) Precursor prepared by homogeneous precipitation; b) Precursor prepared by a conventional precipitation with NH_4HCO_3 solution.

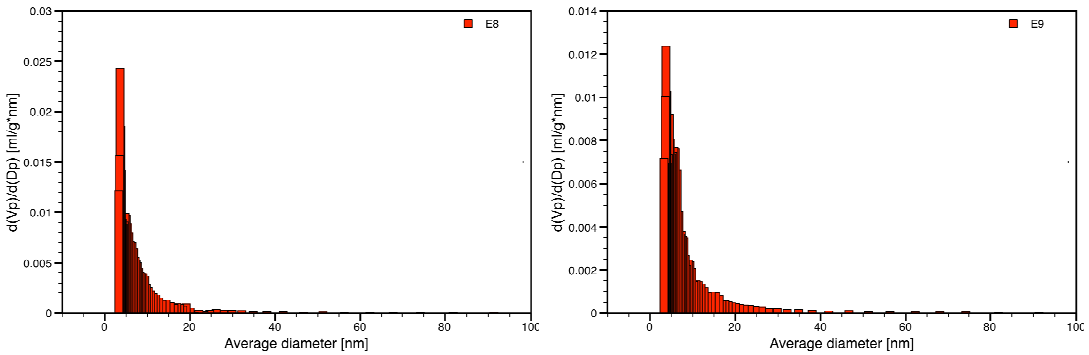

a) b)

Fig. S6. Pore size distributions cerium oxides: a) HP-CeO_2; b) CA-CeO_2

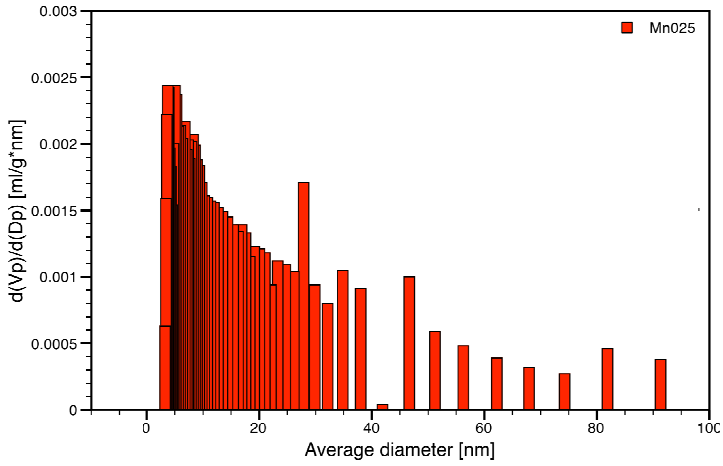

Fig. S7. Pore size distributions – commercial nanoceria MKN-025

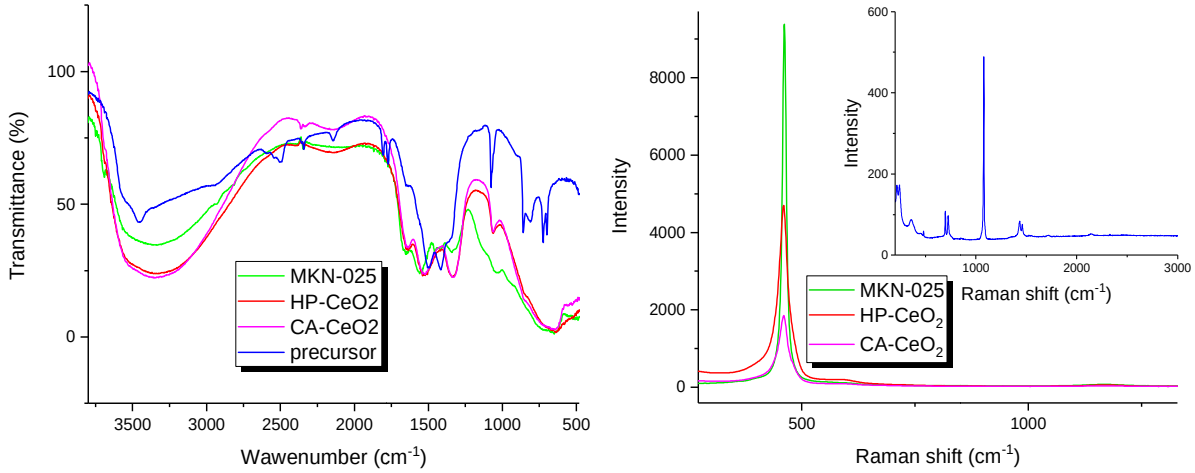

Fig. S7. IR and Raman spectra of the precursor (cerium carbonate) and cerium oxides.

S5. Measurements of the phosphatase-mimetic ability

a) Spectrophotometric determination of the phosphatase – mimetic ability using the standardized test

The standardized phosphatase test ALP-MEG L-500 (Erba Lachema, Brno, Czech Republic) was modified slightly to be applicable for an examination of solid materials. The test utilizes 4-nitrophenyl phosphate as substrate and the production of 4-nitrophenyl phosphate is followed spectrometrically. The intermediate precision (between-day repeatability) of the determination was estimated from the duplicate analyses using the following equation:

$$s_D = \sqrt{\frac{\sum_{i=1}^{k}(D_i - \overline{D})^2}{k-1}}$$

From the series of the duplicate analyses of different cerium oxides (k=11), the relative standard deviation s_D = 2.17% was estimated.

b) HPLC analyses

Concentrations of TPP, NAD and related compounds, as well as their products of dephosphorylation and reaction intermediates, were determined by liquid chromatography using the LaChrom HPLC system (Merck/Hitachi) consisting of the L-7100 pump, the L-7400 variable wavelength UV/Vis detector operating at 240 nm, the Rheodyne 7725i injection valve with 20 µL sampling loop and the Triart Diol-HILIC column (YMC Comp., Kyoto, Japan) 150×3 mm, 5 µm.

Table S2. Mobile phase composition and performance characteristics of the HPLC method

Substrate	Mobile phase	Analyte	LOD (mg/L)	RSD (%)
TPP	acetonitrile/acetate buffer 0.10 mol/L, pH 5.01 67/33 (v/v)	thiamine TMP TPP	3.22 7.72 8.25	9.4 12.6 12.8
NAD	acetonitrile/acetate buffer 0.01 mol/L, pH 5.05 70/30 (v/v)	nicotinamide adenosine NAD	4.43 6.38 7.63	11.4 14.2 13.1

TPP – thiamine pyrophosphate; TMP – thiamine monophosphate; NAD – nicotinamide adenine dinucleotide; LOD – limit of detection; RSD – relative standard deviation of repeatability (n=7)

c) Examinations of the cerium oxide interactions with TPP and NAD

The long-term dephosphorylation experiments were carried out in 20 mL glass vials containing 10 mL of a 0.002 mol/L TPP solution in TRIS buffer (concentration of 0.04 mol/L, pH 7.22). The kinetic experiments were initiated by the addition of a known amount of cerium oxide (typically 0.05 g). The closed glass vials were wrapped in aluminium foil to protect the reaction mixture from sunlight and then agitated on a horizontal shaker with an agitation intensity of 2 rps. At pre-determined time intervals, small amounts (0.1-0.5 mL) of the reaction mixture were removed, acidified with 1 mL of formic acid (1%) and diluted to 5 mL with acetonitrile. Cerium oxide was separated by centrifugation (4000 rpm, 5 min), and the supernatant was analysed immediately by liquid chromatography. Simultaneously, blank experiments were carried out in the same arrangement without cerium oxide. The short-term experiments were carried out in a beaker covered with aluminium foil. Appropriate amounts of the TRIS buffer and TPP stock solution were mixed together to produce a mixture with an initial TPP concentration of 0.002 mol/L, buffer concentration of 0.04 mol/L and pH of 7.22. The mixture was agitated with a magnetic stirrer. The kinetic experiments were initiated by the addition of a known amount of cerium oxide (ranging from 0.5 to 2 g per 100 mL). The liquid chromatographic analyses were performed in a similar way as described above. The mode of agitation was confirmed to not significantly affect the dephosphorylation rate. All the experiments were carried out in an air-conditioned box at 22±1°C.

Interactions of NAD with cerium oxide were examined in an essentially the same arrangement.

d) Quality control and uncertainty estimation

Several kinds of the quality-control (QC) samples were used regularly to check the quality of the chromatographic measurements, such as reagent blanks and in-house reference materials consisting of the analyte solutions daily prepared independently on the calibration standards.

The dephosphorylating experiments (and the experiments examining the interactions of NAD with cerium oxide) were performed in duplicate. A consistency of the experimental data was evaluated by a visual inspection of the dephosphorylating curves. In the case of inconsistency, the whole dephosphorylating experiment was repeated, again in duplicate. The averages from the duplicate measurements were plotted against the reaction time to obtain the dephosphorylating dependencies accompanied by an uncertainty (error bar) expressed as a standard deviation.

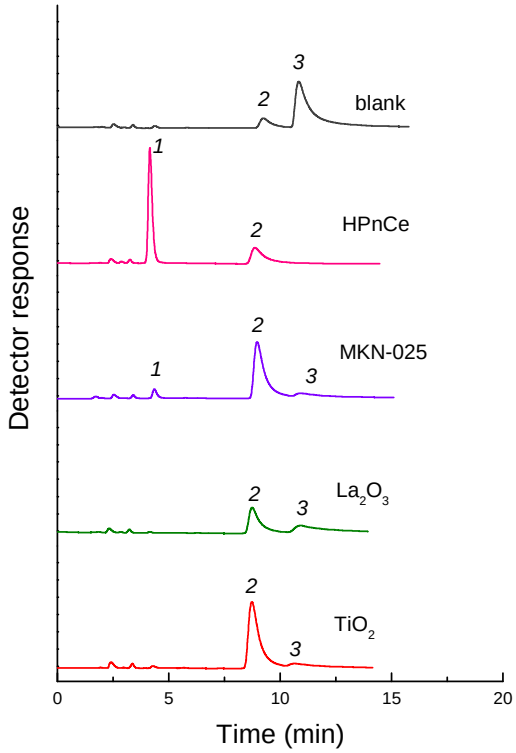

Fig. S8. Dephosphorylation of TPP in the presence various oxides. Initial concentrations of TPP 0.002 mol/L,; 0.04 mol/l TRIS buffer with pH = 7.22. Concentrations of metal oxides 1.0 g/50 mL; equilibrating time 24 hours. Chromatographic conditions: Column YMC-TRIART DIOL-HILIC, 150 × 4.6 mm, 5 µm; mobile phase acetonitrile/ammonium acetate 0.1 mol/L, pH 5.01 (67/33, v/v); detection UV 244 nm. Peak identification: *1* – thiamine; *2* – TMP; *3* – TPP.

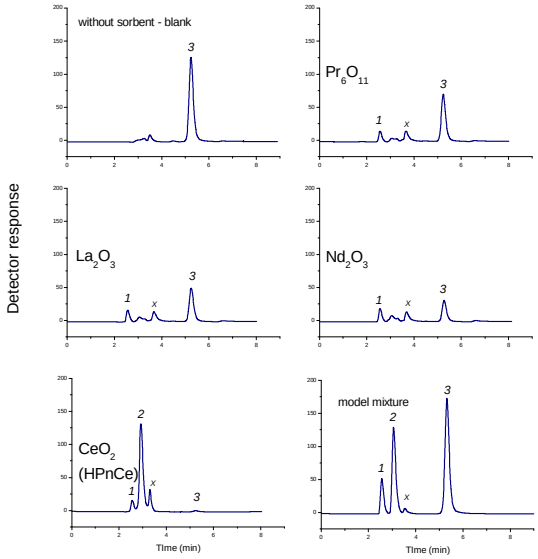

Fig. S9. Decomposition of NAD in the presence REE oxides. Initial concentrations of NAD 0.002 mol/L,; 0.04 mol/l TRIS buffer with pH = 7.22. Concentrations of metal oxides 2.0 g/50 mL; equilibrating time 250 hours. Chromatographic conditions: Column YMC-TRIART DIOL-HILIC, 150 × 4.6 mm, 5 µm; mobile phase acetonitrile/ammonium acetate 0.01 mol/L, pH 5.05 (70/30, v/v); detection UV 244 nm. Peak identification: *1* – nicotinamide; *2* – adenosine; *3* – NAD.

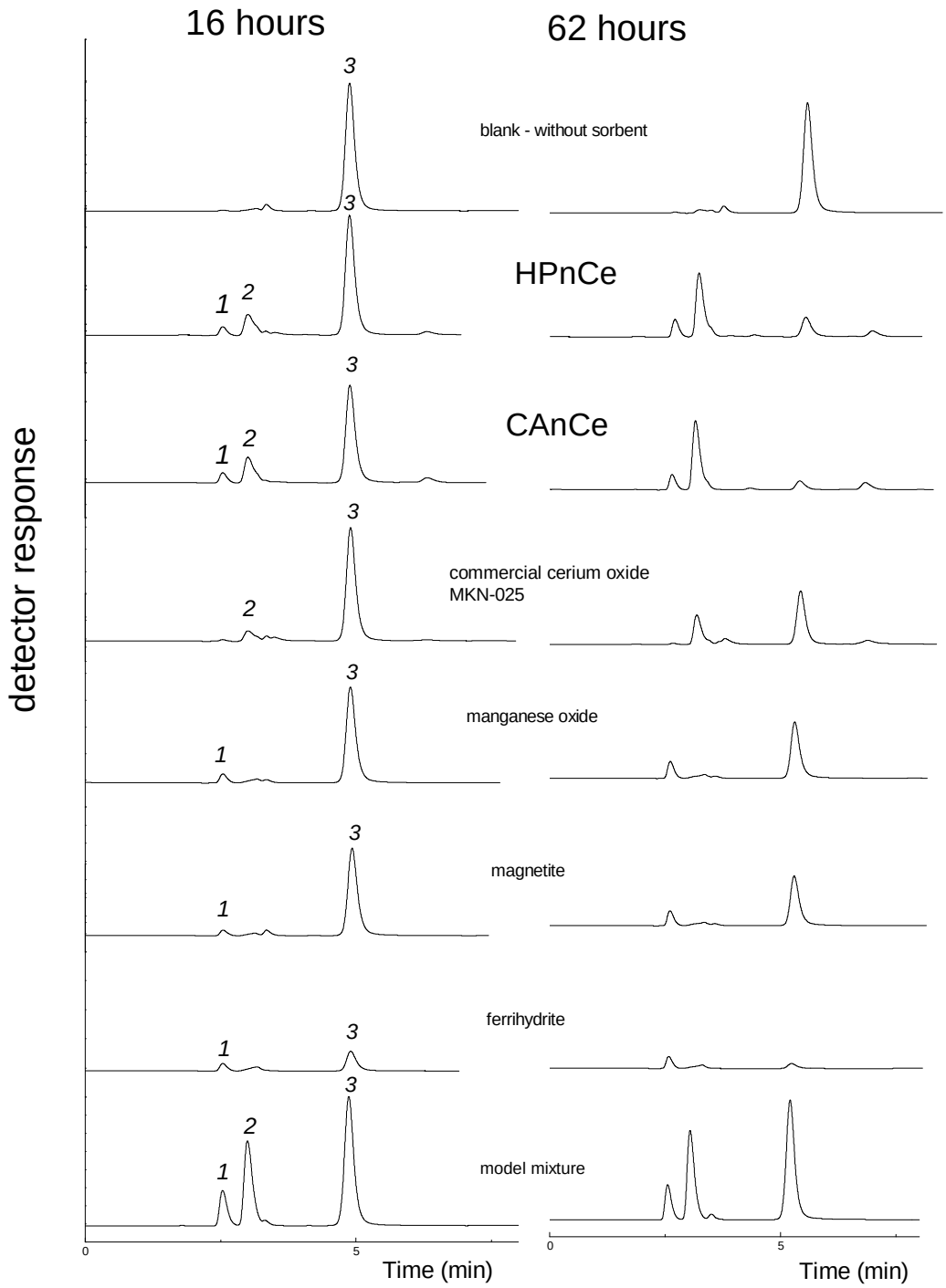

Fig. S10. Decomposition of NAD in the presence of various metal oxides. Initial concentrations of NAD 0.002 mol/L,; 0.04 mol/l TRIS buffer with pH = 7.22. Concentrations of metal oxides 2.0 g/50 mL; equilibrating time 16 hours (left column) and 62 hours (right column). Chromatographic conditions: Column YMC-TRIART DIOL-HILIC, 150 × 4.6 mm, 5 µm; mobile phase acetonitrile/ammonium acetate 0.01 mol/L, pH 5.05 (70/30, v/v); detection UV 244 nm. Peak identification: *1* – nicotinamide; *2* – adenosine; *3* – NAD.

S6. Kinetics of the TPP dephosphorylation

In the first approximation, the dephosphorylation of TMP and thiamine may be described by a set of subsequent pseudo first-order reactions

$$A \xrightarrow{k_1} B \xrightarrow{k_2} C$$

$$-\frac{d\,c_A}{d\,t} = k_1\,c_A \qquad (S1)$$

$$\frac{d\,c_B}{d\,t} = k_1\,c_A - k_2\,c_B \qquad (S2)$$

$$\frac{d\,c_C}{d\,t} = k_2\,c_B \qquad (S3)$$

from which time dependencies for all compounds can be explicitly expressed (assuming that $k_1 \neq k_2$):

$$c_A = c_A^0 \exp(-k_1\,t) \qquad (S4)$$

$$c_B = c_A^0 \frac{k_1}{k_2 - k_1}\,[exp(-k_1\,t) - \exp(-k_2\,t)] \qquad (S5)$$

$$c_C = c_A^0 \left[1 + \frac{k_1 \exp(-k_2 t) - k_2 \exp(-k_1 t)}{k_2 - k_1}\right] \qquad (S6)$$

If $k_1 >> k_2$, then Eq. (S6) may be simplified as follows:

$$c_C = c_A^0\,[1 - \exp(-k_2\,t)] \qquad (S7)$$

The time dependencies for the liberation of thiamine from TPP in the presence of various doses of cerium oxide were evaluated using Eq. (S7); the respective values of the rate constants are listed in the following table:

Table S3. Parameters of the kinetic model for the liberation of thiamine from TPP in the presence of various concentrations of cerium oxide (HPnCe). Initial concentrations of TPP 0.002 mol/L; 0.04 mol/l TRIS buffer with pH = 7.22.

Concentration of cerium oxide (g/L)	Rate constant k_2 (hr^{-1})	Standard error (hr^{-1})	R^2
5	0.0093	0.0046	0.935
10	0.0137	0.0066	0.964
15	0.0213	0.0050	0.975
20	0.0373	0.0054	0.984

S7. Computer simulations

3D computer models of spherical CeO_2 nanoparticle (diameter 2 nm) and thiamine pyrophosphate (TPP) were created using Materials Studio from BIOVIA (formerly Accelrys). In case of nicotinamide adenine dinucleotide (NAD in our study) we used 3D structure provided by Ross Walker (http://research.bmh.manchester.ac.uk/bryce/amber **[R_1], [R_2])**. The RESP technique **[R_3]** was used for calculation of NAD and TPP atoms partial charges. In case of NAD, the RESP charges were taken from library provided by Ross Walker (http://research.bmh.manchester.ac.uk/bryce/amber **[R_1], [R_2]**) For TPP charge parametrization the R.E.D.-IV tools **[R_4]** was used. The necessary QM calculations (QM structure minimisations, molecular electrostatic potential (MEP) calculations) were done using GAMESS **[R_5], [R_6**]. The default, HF/6-31G*, level of theory was used for all charge-related QM calculations and the MEP potential was fitted on Connolly molecular surface. Charges for Ce and O atoms in CeO_2 nanoparticle were taken from the work of Md. Khorshed Alama et al. **[R_7].** The initial oxygen charge value (- 0.2315) was taken as the average from the first column in the Table 6 (0 fs) so the corresponding initial charge value for the cerium atoms was +0.463. With these charges the net charge of the whole nanoparticle was 5.556 so the opposite charge was distributed between all nanoparticle atoms (with uniform relative charge) to neutralize it. The final oxygen and cerium charges was then -0.244119 and 0.437834, respectively. GAFF force field (Generalized Amber Force Field), was used for parameterization of all molecular components **[R_8]** using antechamber routine from Amber14 simulation package **[R_9]**. Missing van der Waals parameters for cerium atoms were taken from MM3 force field **[R_10]**. The initial configurations of TPP/CeO_2 NAD/CeO_2 complexes were created using UCSF Chimera software, which was also used for final visualizations and cluster analysis **[R_11]**. Those complexes were then solvated in TIP3P water (octahedral simulation box, 20 Å thick water shell) and the systems were neutralised by adding one and two Na^+ ions in NAD and TPP case, respectively. First the systems were minimized (10 000 steps with restrained molecular complex, 200 kcal/(mol $Å^2$) restraint), heated (100 ps NVT, 1 fs time step, with restrained molecular complex, 200 kcal/(mol $Å^2$) restraint) to 294 K and finally equilibrated using 55 ns long molecular dynamics simulations (NPT, T = 294 K, P = 0.1 MPa, with restrained atoms of CeO_2 nanoparticle only, 200 kcal/(mol $Å^2$) restraint). The *pmemd.cuda* module from Amber14 package was used for all the above described simulation steps **[R_12]**. Langevin thermostat with collision frequency 2 ps^{-1} was used for all MD runs [**R_13**]. The pressure relaxation time for weak-coupling barostat was 2 ps. Particle mesh Ewald method (PME) was used to treat long range electrostatic interactions under periodic conditions with a direct space cutoff of 10 Angstroms. The same cutoff was used for van der Waals interactions. Last 10 ns part of the trajectory was used (200 frames/configurations analysed) to estimate enthalpic contribution of binding energy using the Molecular Mechanics / Poisson Boltzmann Surface Area (MM-PBSA) methodology. These calculations were accomplished using Adaptive Poisson-Boltzmann Solver "sander.APBS" from Amber14 [**R_14], [R_15**]. The probe radius used for calculation of solvent accessible surface area (SASA) was 1.4 A. Default APBS value a = 0.02508 $kcal*mol^{-1}*A^{-2}$ of cavity surften parametr for calculation of the non-polar solvent contribution ENPOLAR = a*SASA was used. The dielectric constant of the solute was set to

one and in the case of solvent to 80. Cluster analysis was done on 200 frames (configurations) which samples the last 50 ns of simulation.

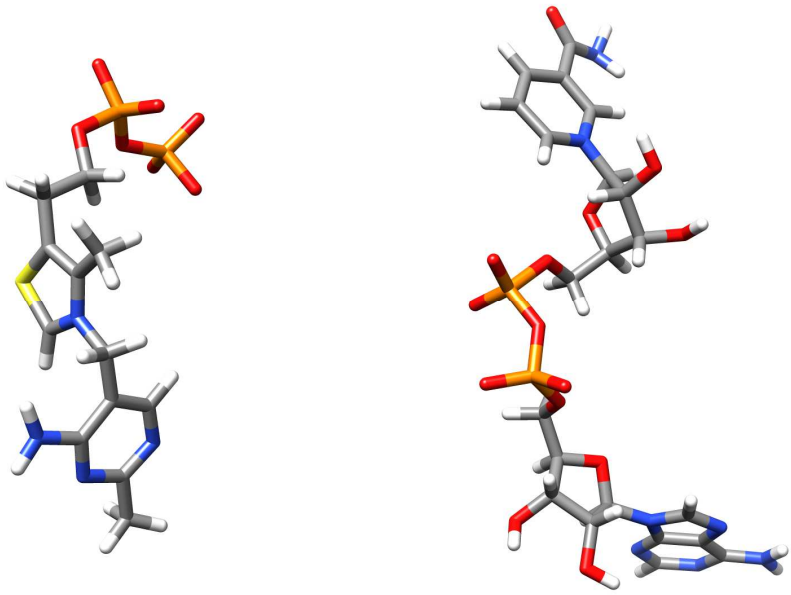

Fig. S11. Computer models of TPP (left) and NAD (right) molecules. Colors: C – gray, H – white, O – red, N – blue, S – yellow, P – orange.

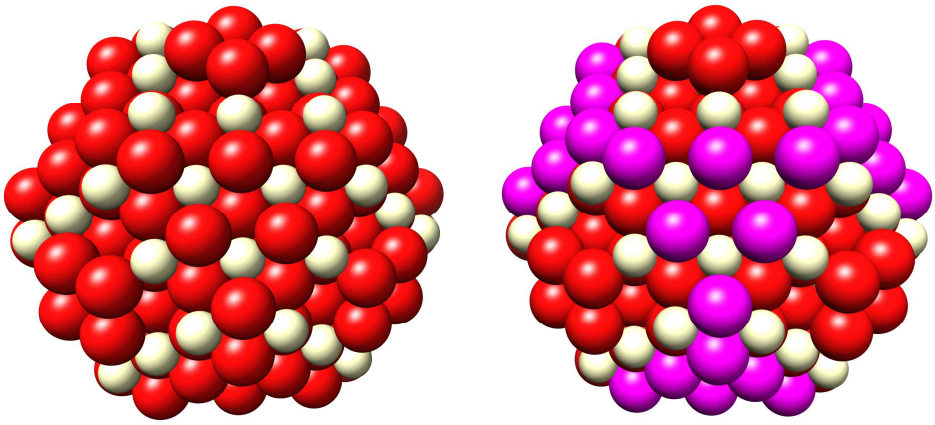

Fig. S12. Computer model of CeO_2 nanoparticle (diameter 2 nm) without (left) and with (right) highlighted binding zones (magenta). Colors: O – red, magenta, Ce – beige.

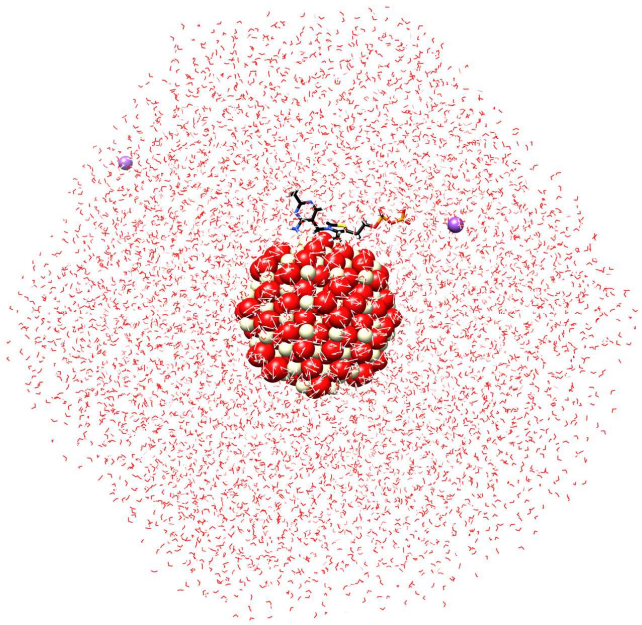

Fig. S13. Complete simulated TPP/CeO_2 system composed of TPP molecule, CeO_2 spherical nanoparticle, water molecules and two Na^+ ions: Colors: C – black, H – white, O – red, N – blue, S – yellow, P – orange, Ce – beige, Na – purple.
.

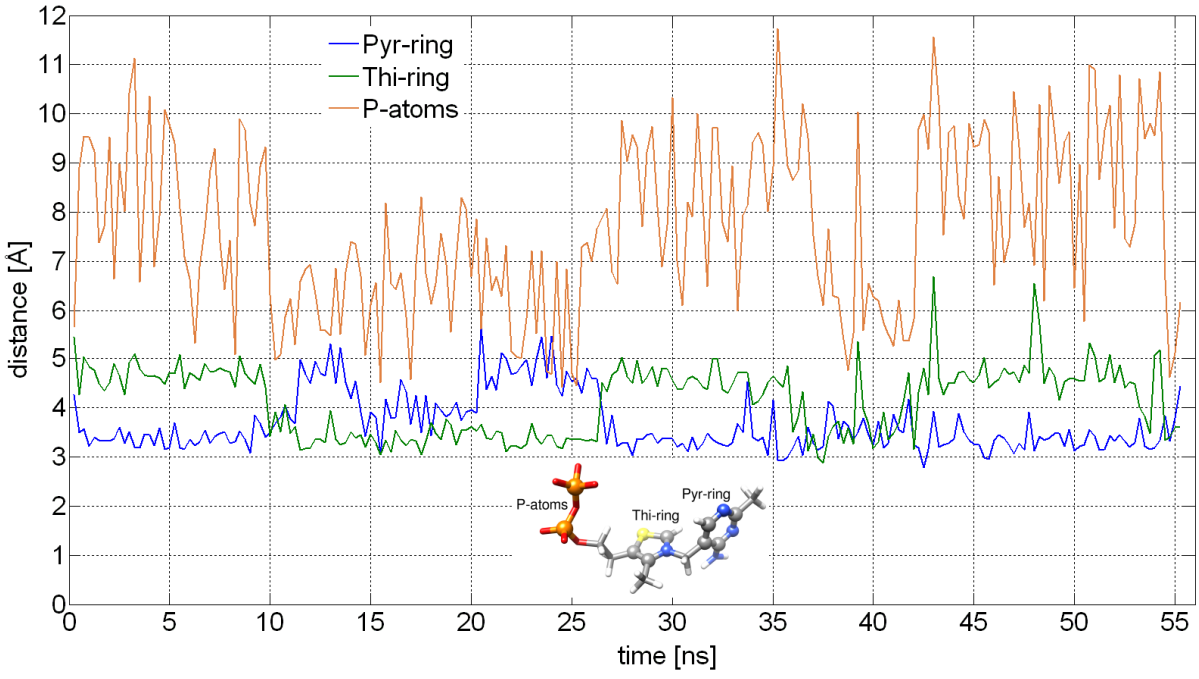

Fig. S14. The evolution of the distance between the CeO_2 nanoparticle surface and rings (Pyrimidine ring: Pyr-ring, Thiazole ring: Thi-ring) or P atoms (orange, ball style) in TPP during the whole NPT simulation. Both rings are represented just by their heavy atoms (atoms represented in ball style). The distance between the given group X of atoms (e.g. given ring) on TPP and CeO_2 surface is the distance between the closest X/CeO_2 atoms (see Video TPP)

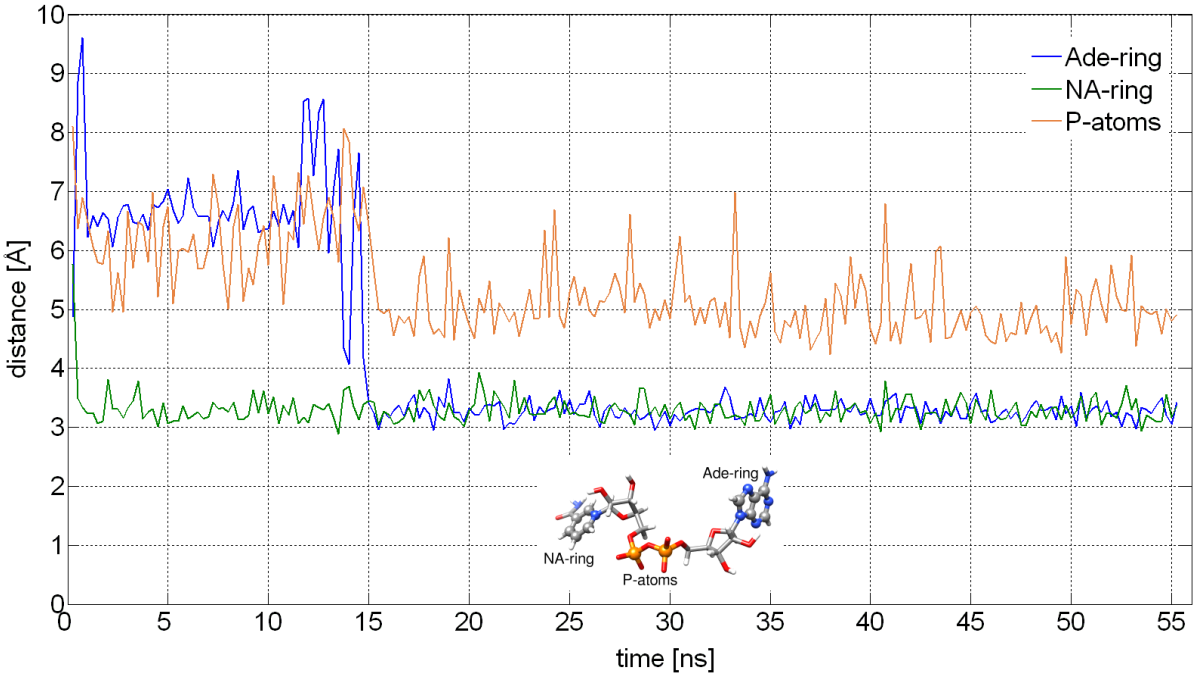

Fig. S15. The evolution of the distance between the CeO_2 nanoparticle surface and rings (Adenine double ring: Ade-ring, Nicotinamide ring: NA-ring) or P atoms (orange, ball style) in NAD during the whole NPT simulation. Both rings are represented just by their heavy atoms (atoms represented in ball style). The distance between the given group X of atoms (e.g. given ring) on NAD and CeO_2 surface is the distance between the closest X/CeO_2 atoms (see Video NAD)

.

Table S3. MM-PBSA estimates of enthalpic contributions to free energies of binding together with all important energetic components. The units are [kcal/mol]. VDW is van der Waals contribution; EEL is electrostatic contribution in vacuum (i.e. without considering solvent); ENP is an estimate for non-polar contribution; EPB is the energetic contribution which arises from electrostatic solvent–solute interaction (desolvation penalty); dH is total enthalpic contribution to free binding energy. dH=VDW+EEL+EPB+ENP.

	TPP	**NAD**
VDW	-18.8809 (1.9708)	-46.5110 (2.4366)
EEL	-2.6326 (2.1955)	-5.7433 (1.4936)
EPB	2.6126 (3.3593)	6.8298 (4.9473)
ENP	-5.8937 (0.4647)	-12.2248 (0.5625)
dH	**-24.7946** (3.9517)	**-57.6494** (5.8504)

The interactions of cerium oxide with TPP and NAD are vizualized in the video files attached as an Electronic supplementary material.

References

[R_1] Walker, R.C, de Souza, M.M., Mercer, I.P., Gould, I.R., Klug, D.R., *Large and Fast Relaxations inside a Protein: Calculation and Measurement of Reorganization Energies in Alcohol Dehydrogenase* J. Phys. Chem. B., 2002, 106 (44), 11658-11665

[R_2] Pavelites, J.J., Gao, J.L., Bash, P.A., Mackerell, A.D., *A Molecular Mechanics Force Field for NAD+, NADH, and the Pyrophosphate Groups of Nucleotides*
J. Comput. Chem. 1997, 18, 221

[R_3] Christopher I. Bayly, Piotr Cieplak, Wendy D. Cornell, and Peter A. Kollman J., *A well-behaved electrostatic potential based method using charge restraints for deriving atomic charges: the RESP model.,* Phys. Chem. 97 (1993) 10269-10280

[R_4] F.-Y. Dupradeau, A. Pigache, T. Zaffran, C. Savineau, R. Lelong, N. Grivel, D. Lelong, W. Rosanski & P. Cieplak, *The R.E.D. tools: Advances in RESP and ESP charge derivation and force field library building,* Phys. Chem. Chem. Phys. 12 (2010) 7821

[R_5] M. W. Schmidt, K. K. Baldridge, J. A. Boatz, S. T. Elbert, M. S. Gordon, J. H. Jensen, S. Koseki, N. Matsunaga, K. A. Nguyen, S. Su, T. L. Windus, M. Dupuis and J. A. Montgomery, *General Atomic and Molecular Electronic Structure System*, J. Comput. Chem., 1993, **14**, 1347-1363.

[R_6] M.S.Gordon, M.W.Schmidt *"Advances in electronic structure theory: GAMESS a decade later" in "Theory and Applications of Computational Chemistry: the first forty years"*, Elsevier, Amsterdam, (2005), pp. 1167-1189

[R_7] Md. Khorshed Alam, Farouq Ahmed, Ryuji Miura, Ai Suzuki, Hideyuki Tsuboi,Nozomu Hatakeyama, Akira Endou, Hiromitsu Takaba, Momoji Kubo, Akira Miyamoto, *Study of reduction processes over cerium oxide surfaces with atomic hydrogen using ultra accelerated quantum chemical molecular dynamics*, Applied Surface Science 257 (2010) 1383–1389

[R_8]. Wang, J.; Wolf, R.M.; Caldwell, J.W.; Kollamn, P.A.; Case, D.A. *Development and testing of a general Amber force field.* J. Comput. Chem., 25, 1157–1174 (2004)

[R_9] D.A. Case, V. Babin, J.T. Berryman, R.M. Betz, Q. Cai, D.S. Cerutti, T.E. Cheatham, III, T.A. Darden, R.E. Duke, H. Gohlke, A.W. Goetz, S. Gusarov, N. Homeyer, P. Janowski, J. Kaus, I. Kolossváry, A. Kovalenko, T.S. Lee, S. LeGrand, T. Luchko, R. Luo, B. Madej, K.M. Merz, F. Paesani, D.R. Roe, A. Roitberg, C. Sagui, R. Salomon-Ferrer, G. Seabra, C.L. Simmerling, W. Smith, J. Swails, R.C. Walker, J. Wang, R.M. Wolf, X. Wu and P.A. Kollman (2014), *AMBER 14*, University of California, San Francisco.

[R_10] A Jenn-Huei Lii, A Norman L. Allinger: *The MM3 force field for amides, polypeptides and proteins* Journal of Computational Chemistry, 12, (1991) , 186-199

[R_11] Pettersen EF, Goddard TD, Huang CC, Couch GS, Greenblatt DM, Meng EC, Ferrin TE. *UCSF Chimera visualization system for exploratory research and analysis.* J Comput Chem. 25(13), (2004), 1605-12

[R_12] W. Goetz; Mark J. Williamson; Dong Xu; Duncan Poole; Scott Le Grand; & Ross C. Walker* *"Routine microsecond molecular dynamics simulations with AMBER - Part I: Generalized Born"*, J. Chem. Theory Comput., 8 (5), (2012), 1542-1555

[R_13]. Wu, X.; Brooks, B.R. *Self-guided Langevin dynamics simulation method.* Chem. Phys. Lett., 381, (2003), 512–518

[R_14] N. A. Baker, D. Sept, S. Joseph, M. J. Holst, J. A. McCammon, Proc. Natl. Acad. Sci. USA, *Electrostatics of nanosystems: Application to microtubules and the ribosome*, 98 (2001) 10037

[R_15] Konecny, Robert; Baker, Nathan A.; McCammon, J. Andrew. *iAPBS: a programming interface to the adaptive Poisson–Boltzmann solver*. Comput. Sci. Disc., 2012, 5(1), 15005–15013.

S7. Mechanisms of the cleavage of the phosphoester bond

Some time ago, Sumaoka et al. [1,2] observed a remarkable acceleration of the hydrolysis of phosphodiesters and DNA in the presence of various cerium compounds. In the acidic solution containing Ce^{4+} cations, the bimetallic cluster with the cerium cations bridged by oxygen atoms, $[Ce_2(OH)_4]^{4+}$, was identified as a catalytically active species accelerating the cleavage of the P-O bonds. The key step is the formation of the 1 : 1 complex with the phosphate group, as shown in the following figure:

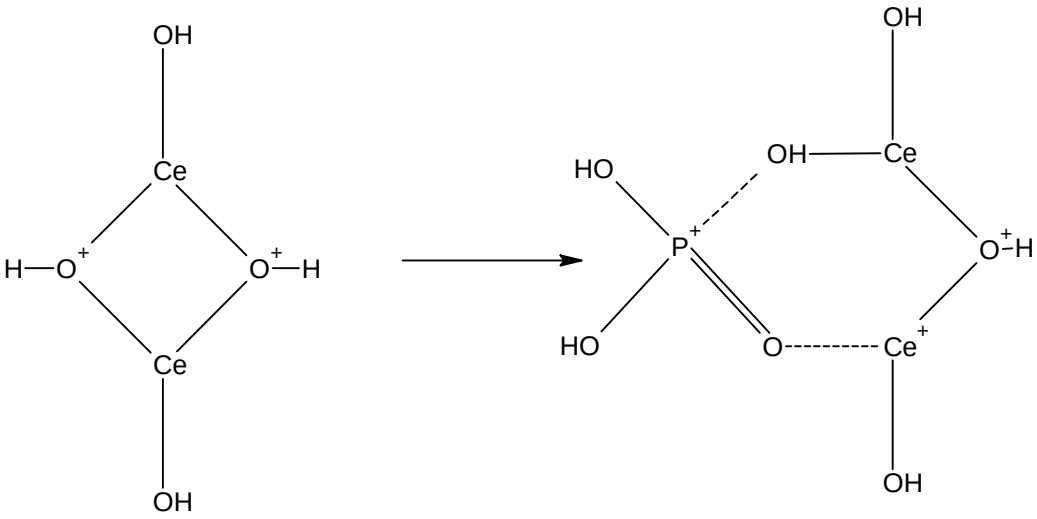

Fig. S16. Bimetalic cluster $[Ce_2(OH)_4]^{4+}$ (left) and its complexation with the phosphate group.

The strong interactions between the Ce^{4+} and a phosphate group were confirmed by Shigekawa et al.[3] with the aid of extended X-ray absorption fine structure spectrometry. They also showed that the *f*-electrons in the Ce ion play a key role in these interactions.

As follows from the XPS analyses, there is a non-negligible amount of oxygen-containing functional groups on the surface of cerium oxide. Undoubtedly, the structures similar to the above mentioned cluster might occur here.

Based on an analogy with the mechanisms effective in the hydrolysis of phosphodiesters in the presence of the Ce^{4+} species, the following mechanism was proposed for the cleavage of the phosphoester bonds on the surface of cerium oxide:

i) Nucleophilic attack of the surface hydroxyl group on the phosphorus atom in the phosphate group in TPP (NAD). The electrophilicity of the P atom is enhanced as a result of the electron-withdrawing effect of the cerium cations.
ii) The pentacoordinate transition state formation.
iii) The cleavage of the P-O bond and liberation of the rest of the molecule as a leaving group.

It should be pointed out that the heterocyclic nitrogen atoms in the TPP (NAD) molecule play also an important role in the interactions of TPP and NAD with cerium oxide because of its ability to interact with the cerium cations [6]. In this way, the TPP or NAD molecules are anchored to the cerium oxide surface, which facilitate the nucleophilic attack of the P atom in the phosphate group.

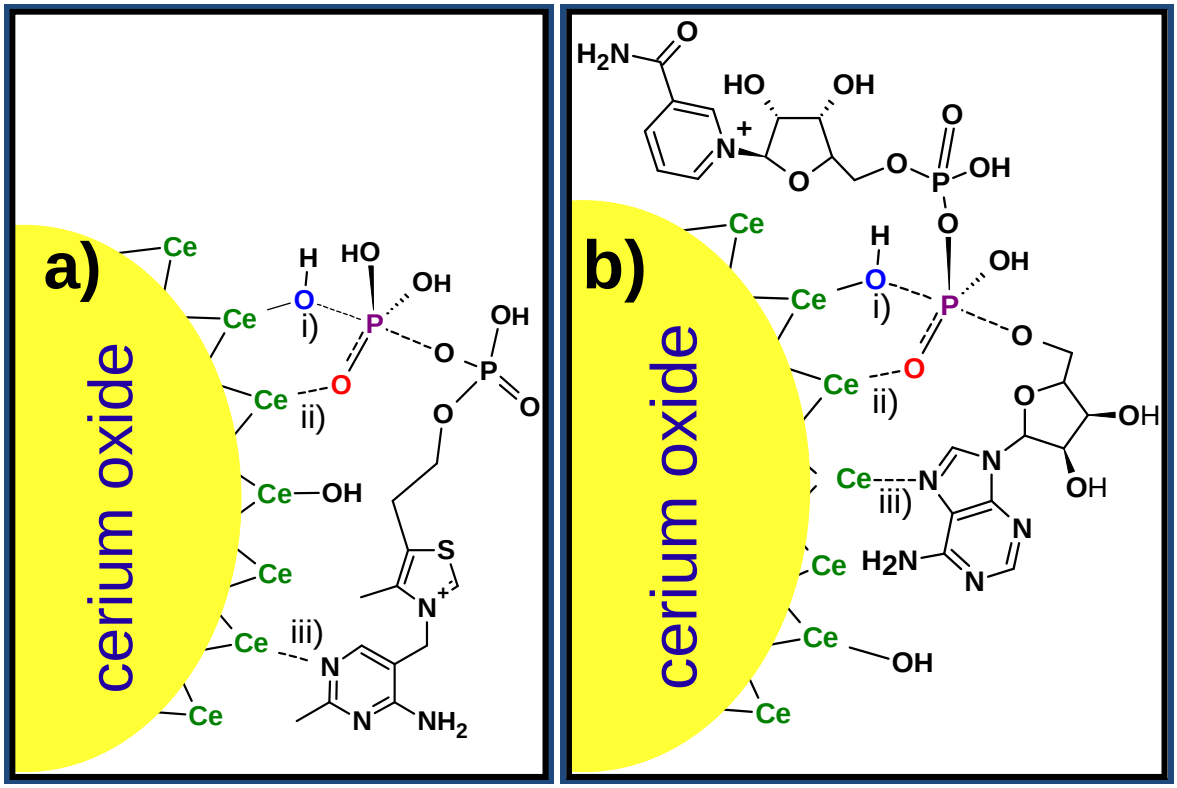

Fig. S17. Possible interactions of TPP (b) and NAD (b) with cerium oxide:. i) Nucleophilic attack of the surface –OH group; ii) Coordination of the phosphate group with cerium cation; iii) Interaction between the heterocyclic nitrogen and cerium cation.

References

[1] Sumaoka, J., Furuki, K., Kojima, Y., Shibata, M., et al., Active Species for Ce(IV)-Induced Hydrolysis of Phosphodiester Linkage in cAMP AND DNA. *Nucleosides, Nucleotides, and Nucleic Acids* 2007.

[2] Shigekawa Hidemi, Ishida Masahiko, Miyake Koji, Shioda Ryu, et al., Extended x-ray absorption fine structure study on the cerium(IV)-induced DNA hydrolysis: Implication to the roles of 4f orbitals in the catalysis. *Appl. Phys. Lett.* 1991, *74*, 460–462.

[3] Tsud, N., Acres, R.G., Iakhnenko, M., Mazur, D., et al., Bonding of histidine to cerium oxide. *J. Phys. Chem. B* 2013, *117*, 9182–9193.